A Combined Synthetic and ab Initio Study of Chiral Oxazaborolidines Structure and Enantioselectivity Relationships

George J. Quallich,* **James F. Blake,*** **and Teresa M. Woodall**

Contribution from Central Research Division, Pfizer Inc, Groton, Connecticut 06340

Received April 11, 1994[⊕]

Abstract: Investigations into the relationship of oxazaborolidine structure to the enantioselectivity obtained in the reduction of prochiral ketones revealed the intrinsic power of the molecular recognition element in the catalytic reduction. This molecular recognition, two-point binding of borane and the ketonic oxygen atom by the oxazaborolidine, assembles a trimolecular complex which provides high enantiomeric excess. Enantiomeric excess was demonstrated to be dependent on the extent to which one oxazaborolidine face was precluded from attaining two-point binding and on nonbonded interactions that developed during formation of the borane–oxazaborolidine complex. As a result, erythro-substituted oxazaborolidines were demonstrated to be useful catalysts for enantioselective reduction of prochiral ketones. Ab initio molecular orbital calculations have been used to locate possible complexes and transition state assemblies that correspond to catalyst–borane and the trimolecular complex on a proposed reduction pathway. Geometry optimizations were carried out at the 3-21G, 6-31G(d), and MP2/6-31G(d) levels of theory. Correlation energies were computed via Møller–Plesset perturbation theory to the second order (MP2). Relative activation energies establish correctly the observed enantioselectivity of the two best oxazaborolidine catalysts in this study. Additionally, the diminished enantioselectivity of *N*-methyl-substituted catalysts was traced to conformational changes in the *exo* transition state. Though the relative energies obtained from the various levels of theory are similar, absolute complexation and activation energies are found to vary considerably with the level of theory employed. The existence of key intermediates was found to depend on the level of theory.

Introduction

Oxazaborolidines have evolved as an important advancement in the enantioselective reduction of prochiral ketones. The pioneering research of Itsuno[1] and Corey[2] has resulted in oxazaborolidines **1** and **2**, respectively, which catalytically provide alcohols of predictable absolute stereochemistry and high enantiomeric excess (ee). Displacement of the resulting chiral hydroxy group by sulfur,[3] nitrogen,[4,5] and carbon nucleophiles[6] provides access to a wide range of products including amino acids, amines, and sulfides. Use of these catalysts highlighted a concern about the availability of unnatural D-amino acid employed in the preparation of oxazaborolidines[7,8] and resulted in a systematic study to provide an understanding of the relationship between the structure and enantioselectivity.[9]

At the outset of our research, geminal diphenyl substituted oxazaborolidines appeared to be optimum for obtaining high ee in catalytic reductions.[10] Geminal diphenyl substitution evolved from Itsuno's survey of amino alcohol derivatives secured from

(X = H, F, Cl, CH₃, CH₃O)
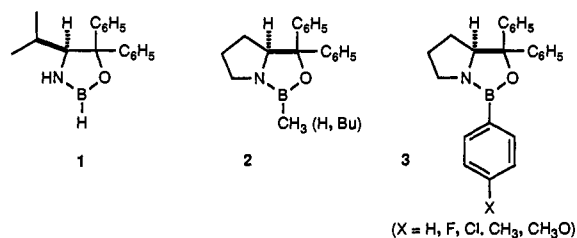
amino acids.[11] Investigations into alternative geminal substitutions of **2**, *i.e.*, isopropyl, α-naphthyl, β-naphthyl, *tert*-butyl, or substituted phenyl, resulted in either a slight improvement or decrease in ee.[12] Jones *et al.* studied the effect of electron density on boron by using substituted phenyl derivatives, catalyst **3**, and concluded that there was no significant electronic effect.[13] Numerous catalysts have been developed recently, but none are superior to the CBS catalyst, **2**.[14] A basic understanding of the relationship between catalyst structure and enantioselectivity in prochiral ketone reductions has not been developed, and the role of the geminal diphenyl substitution in the best catalysts is not well understood.[15b] Consequently, our approach employed ab initio molecular orbital calculations in concert with a systematic synthetic study.

Previous ab initio investigations focused on model systems[15] or employed semiempirical treatments.[16] Our goal was to document the level of theory necessary for reproducing the experimentally determined enantioselectivities and to gain insight into possible

[⊕] Abstract published in *Advance ACS Abstracts,* August 15, 1994.

(1) (a) Hirao, A.; Itsuno, S.; Nakahama, S.; Yamazaki, Y. *J. Chem. Soc., Chem. Commun.* **1981,** 315–17. (b) Itsuno, S.; Hirao, A.; Nakahama, S.; Yamazaki, Y. *J. Chem. Soc., Chem. Commun.* **1983,** 1673–6. (c) Itsuno, S.; Ito, K. *J. Chem. Soc., Perkin Trans. 1* **1984,** 2887–93. (d) Itsuno, S.; Ito, K. *J. Org. Chem.* **1984,** *49,* 555–7. (e) Itsuno, S.; Nakano, M.; Miyazaki, K.; Masuda, H.; Ito, K.; Hirao, A.; Nakahama, S. *J. Chem. Soc., Perkin Trans. 1* **1985,** 2039–44. (f) Itsuno, S.; Ito, K.; Hirao, A.; Nakahama, S. *Bull. Chem. Soc. Jpn.* **1987,** *60,* 395–6.

(2) (a) Corey, E. J.; Bakshi, R. K.; Shibata, S. *J. Am. Chem. Soc.* **1987,** *109,* 5551–52. (b) Corey, E. J.; Bakshi, R. K.; Shibata, S.; Chen, C.-P.; Singh, V. K. *J. Am. Chem. Soc.* **1987,** *109,* 7925–6.

(3) Corey, E. J.; Cimprich, K. A. *Tetrahedron Lett.* **1992,** *33,* 4099–4102.

(4) Chen, P.-C.; Prasad, K.; Repic, O. *Tetrahedron Lett.* **1991,** *32,* 7175–78.

(5) Corey, E. J.; Link, J. O. *J. Am. Chem. Soc.* **1992,** *114,* 1906–08.

(6) Quallich, G. J.; Woodall, T. M. *Tetrahedron* **1992,** *48,* 10239–48.

(7) Brown, H. C.; Ramachandran, P. V. *Acc. Chem. Res.* **1992,** *25,* 16–24.

(8) Kerrick, S. T.; Beak, P. *J. Am. Chem. Soc.* **1991,** *113,* 9708–10.

(9) A preliminary account of this research has been published. Quallich, G. J.; Woodall, T. M. *Tetrahedron Lett.* **1993,** *34,* 4145–48.

(10) Singh, V. K. *Synthesis* **1992,** 605–17.

(11) Itsuno, S.; Ito, K.; Hirao, A.; Nakahama, S. *J. Chem. Soc., Chem. Commun.* **1983,** 469–70.

(12) (a) Corey, E. J.; Link, J. O. *Tetrahedron Lett.* **1989,** *30,* 6275–78. (b) Corey, E. J.; Link, J. O. *J. Org. Chem.* **1991,** *56,* 442–44.

(13) Jones, T. K.; Mohan, J. J.; Xavier, L. C.; Blacklock, T. J.; Mathre, D. J.; Sohar, P.; Jones, E. T. T.; Reamer, R. A.; Roberts, F. E.; Grabowski, E. J. J. *J. Org. Chem.* **1991,** *56,* 763–69.

(14) (a) Martens, J. *Tetrahedron: Asymmetry* **1992,** *3,* 1475–1504. (b) Deloux, L.; Srebnik, M. *Chem. Rev.* **1993,** *93,* 763–84. (c) Kim, Y. H.; Park, D. H.; Byun, I. S. *J. Org. Chem.* **1993,** *58,* 4511–12. (d) Didier, E.; Loubinoux, B.; Tombo, G. M. R.; Rihs, G. *Tetrahedron* **1991,** *47,* 4941–58.

reaction mechanisms, including the existence of various proposed intermediates. Geometry optimizations have been carried out at the 3-21G, 6-31G(d), and MP2/6-31G(d) levels of theory.

Experimental Section

Proton and carbon NMR were recorded on a Brucker 300-MHz spectrometer in the indicated solvents and are reported in ppm relative to $CHCl_3$ or C_6H_6. High-resolution mass spectra were recorded on VG Trio 2000 quadrupole instrument and were mass calibrated using perfluorotributylamine as reference. Air- and moisture-sensitive reactions were performed under nitrogen or argon. Known oxazaborolidines 4,[17] 5,[18] 6,[17] 12,[18] and 13[12] were prepared with trimethylboroxine. Aldrich Sure Seal tetrahydrofuran (THF), 2 M borane–methyl sulfide complex in THF, toluene ACS grade, trimethylboroxine, triphenylboroxine, and butaneboronic acid were employed without further purification or drying.

(4*R-cis*)-2-Methyl-4,5-diphenyl-1,3,2-oxazaborolidine (7). (1*S*,2*R*)-(+)-2-Amino-1,2-diphenylethanol (4.9 g, 22.9 mmol) was suspended in toluene (150 mL) and heated to 80 °C to afford a colorless solution. The reaction mixture was treated in one portion with trimethylboroxine (2.13 mL, 15 mmol) and the heating bath removed. The reaction mixture was stirred for 18 h. Toluene, excess trimethylboroxine, and water were distilled off until only 65 mL remained. The reaction was diluted with toluene (3 × 60 mL), each time distilling until 65 mL remained. After the fourth distillation, the remaining toluene was removed at atmospheric pressure and then under high vacuum to yield the oxazaborolidine (5.15 g, 94%) as a off-white solid: mp 69–70 °C; $\alpha_D = -65°$ (c = 2, toluene); ^{1}H NMR (C_6D_6) δ 7.21–6.68 (m, 10H), 5.54 (d, J = 8 Hz, 1H), 4.48 (d, J = 8 Hz, 1H), 3.02 (bs, 1H), 0.46 (s, 3H); EIMS, M⁺ 237.1324 (calcd 237.1325). Anal. Calcd for $C_{15}H_{16}BNO$: C, 75.98; H, 6.80; N, 5.91. Found: C, 75.88; H, 7.16; N, 5.84.

(4*R-cis*)-2,4,5-Triphenyl-1,3,2-oxazaborolidine (8). (1*S*,2*R*)-(+)-2-Amino-1,2-diphenylethanol (8.252 g, 38.79 mmol) and triphenylboroxine (4.11 g, 12.9 mmol) were combined with toluene (200 mL) and water was removed by the Dean–Stark method for 24 h. The solvents were removed under vacuum and product distilled under vacuum to provide the oxazaborolidine as a thick colorless syrup (9.50 g, 88%): bp 182–85 °C (0.3 mmHg); ^{1}H NMR (C_6D_6) δ 7.90–7.84 (m, 2H), 7.28–6.72 (m, 13H), 5.67 (d, J = 8 Hz, 1H), 4.59 (d, J = 8 Hz, 1H), 3.50 (bs, 1H). Anal. Calcd for $C_{20}H_{18}BNO$: C, 80.29; H, 6.06; N, 4.68. Found: C, 79.99; H, 6.14; N, 4.48.

(4*R-cis*)-2-Butyl-4,5-diphenyl-1,3,2-oxazaborolidine (9). (1*S*,2*R*)-(+)-2-Amino-1,2-diphenylethanol (8.531 g, 40 mmol) and butaneboronic acid (4.077 g, 40 mmol) were combined with toluene (200 mL) and water was removed by the Dean–Stark method for 24 h. The solvents were removed under vacuum, and the product was distilled under vacuum to provide the oxazaborolidine as a colorless oil (10.27 g, 92%): bp 145–46 °C (0.3 mmHg); ^{1}H NMR (CDCl₃) δ 7.38–6.89 (m, 10H), 5.77 (d, J = 8 Hz, 1H), 4.98 (d, J = 8 Hz, 1H), 3.70 (bs, 1H), 1.64–1.42 (m, 4H), 1.08 (t, J = 7 Hz, 2H), 1.00 (t, J = 7 Hz, 3H). Anal. Calcd for $C_{18}H_{22}$-BNO: C, 77.43; H, 8.07; N, 5.18. Found: C, 77.23; H, 7.94; N, 5.02.

(4*R-cis*)-4,5-Diphenyl-1,3,2-oxazaborolidine (10) was prepared by the method of Brown:[18,19] EIMS, M⁺ 223.1159 (calcd. 223.1168).

(4*R-cis*)-2,3-Dimethyl-4,5-diphenyl-1,3,2-oxazaborolidine (11). Trimethylboroxine (0.95 mL, 6.8 mmol) was added to a suspension of (1*S*,2*R*)-(+)-2-(methylamino)-1,2-diphenylethanol (2.27 g, 10 mmol) in toluene (30 mL). The reaction was stirred for 16 h. Toluene, excess trimethylboroxine, and water were distilled off until only 15 mL remained. The reaction was diluted with toluene (3 × 18 mL), each time distilling until 15 mL remained. After the fourth distillation, the remaining toluene was removed at atmospheric pressure and then under high vacuum to yield a white solid (2.48 g, 99%): $\alpha_D = -50.29°$ (c = 1, toluene); mp 86–7 °C; ^{1}H NMR (C_6D_6) δ 7.10 (m, 10H), 5.58 (d, J = 8.5 Hz, 1H), 4.19

(d, J = 8.5 Hz, 1H), 2.28 (s, 3H), 0.49 (s, 3H). Anal. Calcd for $C_{16}H_{18}$-BNO: C, 76.52; H, 7.22, N, 5.58. Found: C, 76.69; H, 7.52; N, 5.66.

Oxazaborolidines 14, 15, 16, 17, and 19 were prepared using the same conditions employed for 7. Note that carbon spectra exclude the 2-methyl carbon signal because of quadrupolar broading in the standard carbon-13 spectra.

2-Methyl-4(*S*)-(2-(methylsulfanyl)ethyl)-1,3,2-oxazaborolidine (14): 83%; ^{1}H NMR (CDCl₃) δ 4.29 (t, J = 9 Hz, 1H), 3.79 (dd, J = 6 Hz, J = 9 Hz, 1H), 3.70 (m, 1H), 3.51 (bs, 1H), 2.49 (t, J = 7 Hz, 2H), 2.10 (s, 3H), 1.75–1.64 (m, 2H), 0.19 (s, 3H); ^{13}C NMR δ 72.3, 54.1, 37.0, 30.7, 15.6.

2-Methyl-4(*S*)-isopropyl-1,3,2-oxazaborolidine (15): 91%; bp 47–48 °C (13 mmHg); ^{1}H NMR (C_6D_6) δ 4.02 (t, J = 9 Hz, 1H), 3.70 (dd, J = 6 Hz, J = 9 Hz, 1H), 2.93 (q, J = 6 Hz, 2H), 1.13 (dq, J = 6 Hz, J = 9 Hz, 1H), 0.58 (d, J = 6 Hz, 3H), 0.52 (d, J = 6 Hz, 3H), 0.26 (s, 3H); ^{13}C NMR (C_6D_6) δ 70.3, 60.9, 33.9, 17.5.

2-Methyl-4(*R*)-phenyl-1,3,2-oxazaborolidine (16): 85%; bp 50–51 °C (0.03 mmHg); mp 37–38 °C; ^{1}H NMR (C_6D_6) δ 7.20–6.95 (m, 5H), 4.21 (m, 2H), 3.79 (dd, J = 5 Hz, J = 8 Hz, 1H), 2.90 (bs, 1H), 0.32 (s, 3H); ^{13}C NMR (CDCl₃) δ 145.0, 128.6, 127.5, 126.1, 75.2, 59.2.

2-Methyl-4(*S*)-*tert*-butyl-1,3,2-oxazaborolidine (17): 82%; ^{1}H NMR (CDCl₃) δ 4.13 (dd, J = 9 Hz, J = 1 Hz, 1H), 3.97 (dd, J = 6 Hz, J = 9 Hz, 1H), 3.30 (dd, J = 9 Hz, J = 6 Hz, 1H), 0.81 (s, 9H), 0.21 (s, 3H); ^{13}C NMR (CDCl₃) δ 68.5, 64.3, 33.5, 21.5.

1,4,10,10-Tetramethyl-3-oxa-5-aza-4-boratricyclo[5.2.1.0.2,6]-decane (19):[20] 91%; ^{1}H NMR (CDCl₃) δ 4.22 (d, J = 8 Hz, 1H), 3.56 (d, J = 8 Hz, 1H), 3.52 (bs, 1H), 1.66 (m, 2H), 1.48 (m, 1H), 1.15 (s, 3H), 1.07 (s, 3H), 0.98 (m, 2H), 0.87 (s, 3H), 0.19 (s, 3H); ^{13}C NMR (CDCl₃) δ 91.4, 64.6, 50.3, 47.9, 46.9, 32.6, 25.5, 23.9, 20.0, 11.3.

Reductions were performed by adding borane–dimethylsulfide complex (2 M in tetrahydrofuran, 14 mmol, 7.0 mL) via syringe pump over 1 h to a tetrahydrofuran (80 mL) solution of oxazaborolidine catalyst (5 mol %) and α-tetralone or pinacolone (20 mmol) at 25 °C. Fifteen minutes after the additions were complete, the reactions were cooled to 0 °C and cautiously quenched with methanol. Isolated yields of products were all ≥90%. Enantiomeric excesses were determined by HPLC with Chiralcel OB for 1,2,3,4-tetrahydro-1-naphthol and 3,3-dimethyl-2-butanol. Product configurations were assigned by the sign of rotation as reported in the literature.[21]

Computational Methods. The ab initio molecular orbital calculations were carried out on a Cray Y-MP2E computer with the Gaussian 92 series of programs.[22] Geometries for the structures were fully optimized by means of analytical energy gradients[23] at the restricted Hartree–Fock level of theory with the split-valence 3-21G[24] and 6-31G(d)[25] basis sets. To provide a basis for evaluating the accuracy of the lower level calculations, model systems were investigated at the 3-21G//3-21G, 6-31G(d)//6-31G(d), and MP2/6-31G(d)//MP2/6-31G(d) levels of theory. The optimized 3-21G structures were used as the starting points for the 6-31G(d) and MP2/6-31G(d) optimizations. All species were fully optimized with no symmetry constraints (*i.e.*, C_1), except for acetone (C_{2v}), *tert*-butyl methyl ketone (C_s), and borane (D_{3h}). Electron correlation energies were computed via second-order Møller–Plesset perturbation theory with the 6-31G(d) basis set.[26]

Vibrational frequencies were calculated at the 3-21G level for all stationary structures.[27] The existence of transition states or minima was confirmed by the presence of either one or zero negative eigenvalues in the analytical second-derivative matrix. Given the similarity of all the analogous structures (*vide infra*), and the imposing computational

(15) (a) Nevalainen, V. *Tetrahedron: Asymmetry* **1991**, *2*, 63–74. (b) Nevalainen, V. *Tetrahedron: Asymmetry* **1991**, *2*, 429–35. (c) Nevalainen, V. *Tetrahedron: Asymmetry* **1991**, *2*, 827–42. (d) Nevalainen, V. *Tetrahedron: Asymmetry* **1991**, *2*, 1133–55. (e) Nevalainen, V. *Tetrahedron: Asymmetry* **1992**, *3*, 921–32. (f) Nevalainen, V. *Tetrahedron: Asymmetry* **1992**, *3*, 933–45. (g) Nevalainen, V. *Tetrahedron: Asymmetry* **1992**, *3*, 1441–53. (h) Nevalainen, V. *Tetrahedron: Asymmetry* **1992**, *3*, 1563–72. (i) Nevalainen, V. *Tetrahedron: Asymmetry* **1993**, *4*, 1597–1602.
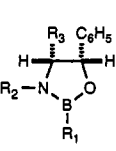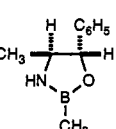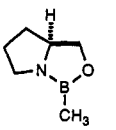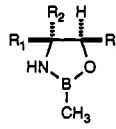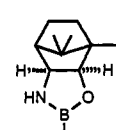
(16) Jones, D. K.; Liotta, D. C. *J. Org. Chem.* **1993**, *58*, 799–801.

(17) Brooks, C. J. W.; Middleditch, B. S.; Anthony, G. M. *Org. Mass Spectrom.* **1969**, *2*, 1023–32.

(18) Joshi, N. N.; Srebnik, M.; Brown, H. C. *Tetrahedron Lett.* **1989**, *30*, 5551–54.

(19) Quallich, G. J.; Woodall, T. M. *Syn Lett.* **1993**, *12*, 929–30.

(20) Chittenden, R. A.; Cooper, G. H. *J. Chem. Soc. C* **1970**, 49–54.

(21) (a) Jacobus, J.; Majerski, Z.; Mislow, K.; Schleyer, P. v. R. *J. Am. Chem. Soc.* **1969**, *91*, 1998–2000. (b) Davies, A. G.; White, A. M. *J. Chem. Soc.* **1952**, 3300–303.

(22) Frisch, M. J.; Trucks, G. W.; Head-Gordon, M.; Gill, P. M. W.; Wong, M. W.; Foresman, J. B.; Johnson, B. G.; Schlegel, H. B.; Robb, M.; Replogle, E. S.; Gomperts, R.; Andres, J. L.; Raghavachari, K.; Binkley, J. S.; Gonzalez, C.; Martin, R. L.; Fox, D. J.; DeFrees, D. J.; Baker, J.; Stewart, J. J. P.; Pople, J. A. Gaussian 92 Version C, Pittsburgh, PA, Gaussian, Inc., 1992.

(23) Schlegel, H. B. *J. Comput. Chem.* **1982**, *3*, 214–18.

(24) Binkley, J. S.; Pople, J. A.; Hehre, W. J. *J. Am. Chem. Soc.* **1980**, *102*, 939–47.

(25) Francl, M. M.; Pietro, W. J.; Hehre, W. J.; Binkley, J. S.; Gordon, M. S.; DeFrees, D. J.; Pople, J. A. *J. Chem. Phys.* **1982**, *77*, 3654–65.

(26) Møller, C.; Plesset, M. S. *Phys. Rev.* **1934**, *46*, 618–22. Pople, J. A.; Binkley, J. S.; Seeger, R. *Int. J. Quantum Chem. Symp.* **1976**, *10*, 1–19.

(27) Pople, J. A.; Krishnan, R.; Schlegel, H. B.; Binkley, J. S. *Int. J. Quantum Chem., Quantum Chem. Symp.* **1979**, *13*, 225–41.

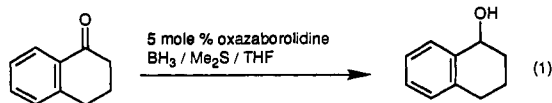**Table 1.** Enantiomeric Excess Obtained with Oxazaborolidine-Catalyzed Reduction of α-Tetralone (Pinacolone)

Entry	absolute configuration	%ee
4 $R^1 = R^2 = R^3 = CH_3$	S	60
	S	74*
5 $R^1 = C_6H_5$; $R^2 = R^3 = CH_3$	S	36
6 $R^1 = R^3 = CH_3$; $R^2 = H$	S (S)	80 (82)
7 $R^1 = CH_3$; $R^2 = H$; $R^3 = C_6H_5$	S (S)	94 (88)
8 $R^1 = R^3 = C_6H_5$; $R^2 = H$	S	88
9 $R^1 = Bu$; $R^2 = H$; $R^3 = C_6H_5$	S	90
10 $R^1 = R^2 = H$; $R^3 = C_6H_5$	S	86
11 $R^1 = R^2 = CH_3$; $R^3 = C_6H_5$	S	0
	S	30*
12	S	2
13	R	78
14 $R^1 = CH_3S(CH_2)_2$; $R^2 = R^3 = H$	R	36
15 $R^1 = (CH_3)_2CH$; $R^2 = R^3 = H$	R	54
16 $R^1 = R^3 = H$; $R^2 = C_6H_5$	S	56
17 $R^1 = (CH_3)_3CH$; $R^2 = R^3 = H$	R	70
18 $R^1 = (CH_3)_3CH$; $R^2 = H$; $R^3 = C_6H_5$	R	82
19	R	80

All reductions were conducted in THF at 25°C employing borane as the reductant with 5 mole % catalyst unless *, then a stoichiometric amount of oxazaborolidine was employed.

demands, we have deferred computation of the vibrational frequencies for the 6-31G(d) and MP2/6-31G(d) structures.

Results and Discussion

Experimental Investigation. The synthetic approach evaluated substituents on the carbon, boron, and nitrogen atoms of the oxazaborolidine ring. Dependence of catalyst structure to the enantioselectivity was assessed by reduction of α-tetralone, eq 1.

$$\text{5 mole \% oxazaborolidine} \quad \text{BH}_3 / \text{Me}_2\text{S} / \text{THF}$$ (1)

The investigation began with ephedrine, pseudoephedrine, and prolinol, which were converted into the corresponding oxazaborolidines with trimethylboroxine.[28] Enantiomeric excesses obtained in the reduction of α-tetralone with 5 mol % of these catalysts are documented in Table 1 (catalysts 4, 12, and 13). Catalysts derived from ephedrine and prolinol gave the highest ee's: 60% and 78%, respectively. Stoichiometric use of the ephedrine oxazaborolidine 4 resulted in higher ee and provided some insight into the catalytic efficiency of enantioselective reduction (Table 1). From this preliminary study, we hypothesized that blocking one face of the oxazaborolidine was critical in securing a high ee (catalysts 4 and 13, Table 1). An erythro diphenyloxazaborolidine was chosen to validate this premise, as one face of the catalyst is effectively shielded due to the orthogonal arrangement of the phenyl substituents in relation to the oxazaborolidine ring (*cf.* Figure 1). Good enantiomeric excess was obtained with any boron

substituent in this erythro diphenyl series, catalysts 7–10 (Table I), in contrast to ephedrine.[29] A series of catalysts derived from amino acids was evaluated to determine whether the face of the oxazaborolidine could be effectively shielded by a single substituent on the carbon atom proximal to the nitrogen atom that coordinates borane.[2a] The trend observed for catalysts 14–17 (Table 1) reflects the *A* values with the *tert*-butyl substituent yielding a 70% ee. The erythro *tert*-butyl/phenyl system 18 did not provide a better enantiomeric excess compared to the diphenyl series 7. Thus, the primary requirement of a good catalyst was to completely block one face of the oxazaborolidine.

Alkyl substitution on the nitrogen of the oxazaborolidine proved to be detrimental to the enantiomeric excess. A methyl group on nitrogen in the diphenyl catalyst, 11, afforded no selectivity (*i.e.*, 0% ee). In this case 20% of the α-tetralone remained on workup employing standard reduction conditions.[30] On the basis of this trend, catalyst derived from norephedrine should and did afford a higher ee than the ephedrine oxazaborolidine, catalyst 6 *vs* 4. Employing a stoichiometric quantity of oxazaborolidine 4 and 11 mitigates noncatalyzed reduction in the ephedrine-based system, but not in the erythro diphenyl case. Similarly the camphor *N*-H-oxazaborolidine 19 provided higher ee when compared to what has been reported for the *N*-alkyl catalyst.[31] Thus nonbonded interactions that develop between the alkyl nitrogen and proximal (C4) carbon substituents resulted in increased noncatalyzed reduction of the ketone by free borane, due to retarded complexation of borane by the oxazaborolidine and/or unselective reduction by the catalyst. Both of these effects are considered in the computational section below. Therefore, the erythro-substituted oxazaborolidines tolerate a variety of substituents on boron but not on nitrogen.

Ab Initio Calculations. 1. Borane Adducts. In the mechanism proposed by Corey, the oxazaborolidine forms adduct 20 with borane, as shown in Scheme 1. A single-crystal X-ray diffraction study supports the existence of this borane adduct.[32] The adduct is thought to complex the ketonic species with the "large" substituent of the ketone in an *exo* fashion to the oxazaborolidine ring (Scheme 1). The hydride transfer is then considered to continue through a "boat-like" transition state assembly.[2] This model is capable of predicting the absolute configuration of the product.

The ab initio molecular orbital calculations were carried out in order to determine the existence of various intermediates on the proposed reduction pathway and the factors responsible for the observed enantioselectivities. The first issue addressed through the computations was generation of the borane adducts of oxazaborolidines 6 and 7. Borane coordination was computed for both *cis* and *trans* geometries with respect to the substituent on the carbon that is proximal (C4) to the coordinating nitrogen (methyl or phenyl of oxazaborolidines 6 and 7, respectively). The lowest energy optimized structures for oxazaborolidines 6 and 7 and the corresponding borane adducts are illustrated in Figure 1. Total and relative energies for all species are recorded in Table 2. At the 3-21G level, the *trans* coordination of borane to 6 and 7 is favored over the *cis* by 7.52 and 11.33 kcal/mol (Table 2). The difference between *trans* and *cis* coordination energies decreases at the 6-31G(d)//6-31G(d) level to 6.51 and 10.05 kcal/mol. Correlation energy corrections have a minor effect on the relative energy differences with *trans* and *cis*

(28) Mathre, D. J.; Jones, T. K.; Xavier, L. C.; Blacklock, T. J.; Reamer, R. A.; Mohan, J. J.; Jones, E. T. T.; Hoogsteen, K.; Baum, M. W.; Grabowski, E. J. J. *J. Org. Chem.* **1991**, *56*, 751–62.
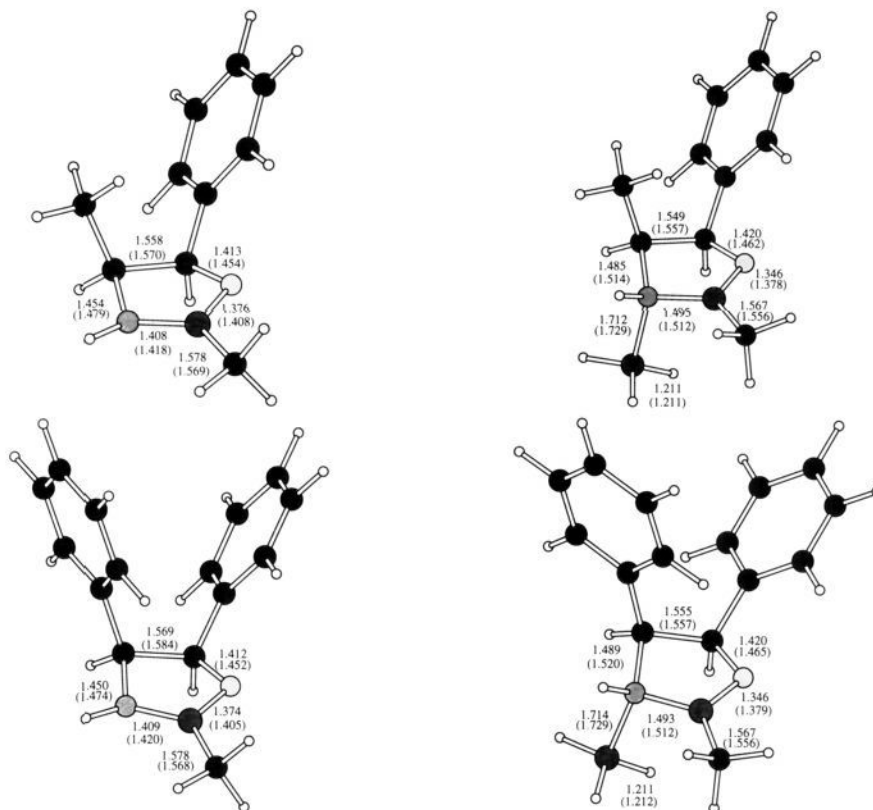
(29) As observed previously, ref 2b, the *B*-H-oxazaborolidines were not as stable as the alkyl derivatives. Thus higher ee's were obtained by preparing the *B*-H oxazaborolidines *in situ*. For example, an 88% ee was secured with catalyst 10 when the oxazaborolidine was isolated and 94% ee when formed *in situ*.

(30) See Experimental Section for standard reaction conditions.

(31) Reduction of acetophenone with the *B*-H analog of 19 afforded an 80% ee while the following authors report a 73% ee when this *B*-H oxazaborolidine was *N*-alkyl substituted. Tanaka, K.; Matsui, J.; Suzuki, H. *J. Chem. Soc., Chem. Commun.* **1991**, 1311–12.
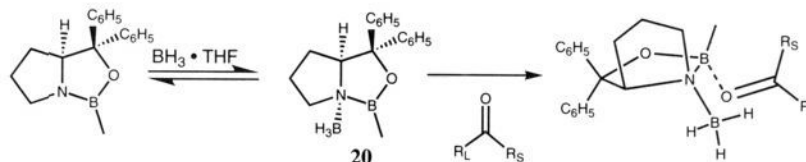
(32) Corey, E. J.; Azimioara, M.; Sarshar, S. *Tetrahedron Lett.* **1992**, *24*, 3429–30.

Figure 1. 6-31G(d) and 3-21G, in parentheses, optimized geometries for **6** (top) and **7** (bottom) and the corresponding borane adducts (bond lengths in angstroms throughout).

Scheme 1

coordination energies for **6** and **7** computed to be 6.51 and 9.28 kcal/mol at the MP2/6-31G(d)//6-31G(d) level. The preference for the *trans* coordination results from the greater steric repulsion in the *cis* form, caused by the interaction of the coordinating borane unit with the C4 substituent of **6** or **7**. The increased preference for *trans* coordination of borane in **7** relative to **6** (2.77 kcal/mol at the MP2/6-31G(d)//6-31G(d) level) is due to the increased steric crowding of the phenyl substitution at C4 of **7** in the *cis* form.

The reported trends in complexation energies are analogous to those observed by LePage and Wiberg in a study of Lewis acid coordination of aldehydes and ketones.[33] These authors found that the coordination energy doubled on going from 6-31G(d)//6-31G(d) to MP2/6-31G(d)//6-31G(d) and that the relative 3-21G//3-21G energies were similar to the MP2/6-31G(d)//6-31G(d) results. The agreement between the 3-21G and MP2/6-31G(d) results is most likely due to fortuitous cancelation of errors in the basis sets and correlation energy corrections. While the relative energies appear to be rather well converged when moving to higher levels of theory, considerable variation in the computed absolute coordination energies remains. On going from the 3-21G//3-21G to the 6-31G(d)//6-31G(d) level of theory, an average loss of *ca.* 8 kcal/mol in coordination energy for all adducts formed is predicted. From the MP2/6-31G(d)//6-31G-(d) calculation, there is a correction in the opposite direction

(33) LePage, T. J.; Wiberg, K. B. *J. Am. Chem. Soc.* **1988**, *110*, 6642–50.

from the 6-31G(d)//6-31G(d) results of *ca.* 14 kcal/mol toward more negative coordination energies. The effects of moving to higher levels of theory (*i.e.*, MP3) have not been explored due to the imposing computational demands. However, based upon experience and prior investigations,[33] we can speculate that the relative energies would change only slightly. The geometries of **6** and **7** and their corresponding borane adducts are, as one would expect, very similar (Figure 1). Borane coordination leads to pyramidalization of the oxazaborolidine nitrogen; this is reflected in the lengthening of the adjacent oxazaborolidine N–B and N–C bonds from 1.418 to 1.512 Å and from 1.479 to 1.514 Å for **6** (3-21G//3-21G). Similar changes are noted upon coordination of borane to **7** (Figure 1). Given the large preference for *trans* coordination of borane over *cis*, only the *trans* adducts of **6** and **7** would be important in considering the catalytic reduction mechanisms.

2. Catalyst Ketone Complexes. Using the Corey model as a guide, four complexes of *tert*-butyl methyl ketone (pinacolone) with the borane adducts of **6** and **7** were located at the 3-21G//3-21G level of theory, as illustrated in Figure 2. *tert*-Butyl methyl ketone was chosen as the most tractable protypical ketone, though the results obtained herein should be extensible to other systems of interest (*e.g.*, α-tetralone). In all cases, the ketone complexes in an *anti* fashion (with respect to the *tert*-butyl group) to the boron of the oxazaborolidine ring, which is consistent with prior ab initio investigations.[33] These complexes are deep minima

Table 2. Electronic Energies (hartrees) and Relative Energies (kcal/mol)

| species	3-21G//3-21G	E_{rel}[a]	6-31G(d)//3-21G	E_{rel}[a]	6-31G(d)//6-31G(d)	E_{rel}[a]	MP2/6-31G(d)//6-31G(d)	E_{rel}[a]	MP2/6-31G(d)//MP2/6-31G(d)	E_{rel}[a]
borane	-26.23730170		-26.39000677		-26.39000740		-26.46422840		-26.46424379	
tert-butyl methyl ketone	-307.34983545		-309.06169679		-309.06292624		-310.02303250			
acetone	-190.88722124		-191.96138328		-191.96223634		-192.52159985		-192.52390508	
6	-537.95306050		-540.93196079		-540.93565860		-542.62570270			
7	-727.39618990		-731.43959062		-731.44337470		-733.76060940			
21	-348.50475091		-350.42303000		-350.42607799		-351.49108915		-351.49322297	
11	-766.20849525									
6-BH₃ (*trans*)	-564.22620440	-22.49	-567.34428820	-14.01	-567.34825848	-14.18	-569.13463570	-28.05		
6-BH₃ (*cis*)	-564.21421240	-14.97	-567.33353998	-7.26	-567.33789160	-7.67	-569.12426190	-21.54		
7-BH₃ (*trans*)	-753.66804090	-21.68	-757.85000602	-12.81	-757.85437060	-13.17	-760.26844750	-27.37		
7-BH₃ (*cis*)	-753.64999110	-10.35	-757.83350153	-2.45	-757.83834880	-3.12	-760.25366970	-18.09		
21-BH₃ (*trans*)	-374.77883192	-23.08	-376.83580500	-14.29	-376.83920675	-14.51	-378.00064798	-28.45	-378.00372502	-29.03
11-BH₃ (*trans*)	-792.47702369	-19.60								
11-BH₃ (*cis*)	-792.45988192	-8.84								
6 (*exo*) transition state	-871.57908560	-24.40	-876.38348292	0.11	-876.38813338	0.29	-879.16511950	-32.73		
6 (*endo*) transition state)	-871.58255995	-26.58	-876.38179222	1.17	-876.38711058	0.93	-879.16350280	-31.71		
7 (*exo*) transition state	-1061.02245700	-24.55	-1066.88975245	0.97	-1066.89486962	0.90	-1070.30058090	-33.08		
7 (*endo*) transition state	-1061.02267086	-24.69	-1066.88512182	3.87	-1066.89045950	3.67	-1070.29639740	-30.45		
21 (*exo*) transition state	-565.66760227	-24.05	-568.77475995	-0.21	-568.77875183	-0.27	-570.52435607	-29.77	-570.52689809	-28.57
21 (*endo*) transition state	-565.67243949	-27.09	-568.77444354	-0.01	-568.77870155	-0.24	-570.52525901	-30.33	-570.52845816	-29.55
11 (*exo*) transition state	-1099.81938457	-14.90								
11 (*endo*) transition state	-1099.82439253	-18.05								
6 (*exo*) complex	-871.59114553	-31.97	-876.39757497	-8.73						
6 (*endo*) complex	-871.59675153	-35.49	-876.39910544	-9.69						
7 (*exo*) complex	-1061.03435510	-32.02	-1066.90358123	-7.71						
7 (*endo*) complex	-1061.03788450	-34.24	-1066.90404866	-8.00						
21 (*exo*) complex	-565.67687442	-29.87	-568.78621117	-7.40					-570.53180817	-31.65
21 (endo) complex	-565.68217318	-33.19	-568.78726413	-8.06					-570.53501758	-33.66
11 (*exo*) complex	-1099.83516671	-24.81								
11 (*endo*) complex	-1099.84145569	-28.75								

[a] Energies are relative to the corresponding catalyst, borane, and ketone reactants. **Bold-faced** numbers refer to species listed in Table 1 and Figure 3.

on the 3-21G potential energy surface; the relative energy of the complex of 7 is -10.34 kcal/mol for the *exo* approach (Chart 1), relative to the corresponding borane adduct (Figure 1). Likewise, the *endo* attack of the ketone is also a deep minima (-12.56 kcal/mol) at the 3-21G level of theory. The ketone complexes of the borane adduct of 6 are at -9.48 and -13.00 kcal/mol, respectively, for the *exo* and *endo* pathways at the 3-21G//3-21G level of theory. There is a clear preference for the *endo* mode of complexation for the borane adducts of both 6 and 7. The inversion of *exo* and *endo* complexes was not considered; given the similarities in complexation energies and geometries to other Lewis acid complexes, barriers of *ca.* 10 kcal/mol or more were anticipated,[33] which precludes interconversion of the two forms. Characteristics of the tighter *endo* complexes are shorter oxazaborolidine boron to carbonyl oxygen (B---O=C) distances, and smaller B---O=C angles. The B---O=C distance for the *endo* complex of 6 is 1.629 Å, which is 0.041 Å shorter than that in the corresponding *exo* complex and is the shortest among the catalyst–ketone complexes studied. The same distance is computed to be 1.636 Å for the *endo* complex of 7, while the *exo* distance is again predicted to be longer at 1.665 Å. The B---O=C angles for the *exo* complexes of 6 and 7 are 144.1° and 143.8°. The equivalent angles for the *endo* complexes of 6 and 7 are 138.9° and 140.0°. Complexation of the ketone appears to have a relatively minor effect on most of the geometrical parameters of the borane adducts. The most striking geometrical change among all the complexes is the pyramidalization of the oxazaborolidine boron (N3–B2–O1–CH₃ torsion) for both 6 and

7, which is distorted from a planar arrangement in the borane adduct to *ca.* 130° in the ketone complexes.

Surprisingly, no analogous ketone complexes at the 6-31G-(d)//6-31G(d) level of theory were located. In attempting to locate possible ketone complexes, analytical energy gradients from the 3-21G calculations were used as initial estimates for the 6-31G-(d) optimizations. Despite repeated attempts, employing a variety of optimization schemes and starting geometries, no stable minima at the 6-31G(d)//6-31G(d) level of theory for the ketone complexes with the borane adducts of either 6 or 7 were located. Clearly, the inclusion of d-type polarization functions has profound effects on the computed geometries and energies of these catalyst–ketone complexes. Insight into this dilemma is gained by examining the relative energies in Table 2. On going from the 3-21G//3-21G to the 6-31G(d)//3-21G level, an increase in complexation and activation energies of *ca.* 15 kcal/mol was found for all structures. This implies that the energies of most stable complexes at the 3-21G//3-21G level (*cf.* the *endo* complex of 6) would be *ca.* 5 kcal/mol above those of the reactants (borane adduct of 6) at the 6-31G(d)//6-31G(d) level. This may explain the difficulty in attempting to characterize the borane adduct ketone complexes at the 6-31G(d)//6-31G(d) level of theory. Further inspection of Table 2 reveals that one would expect a greater compensating correction on moving to correlated geometries (*i.e.*, MP2/6-31G(d)//MP2/6-31G(d)). Thus, one would anticipate that complexes would be located at the MP2/6-31G-(d)//MP2/6-31G(d) level of theory.

3. Model Oxazaborolidines. To probe this issue further,
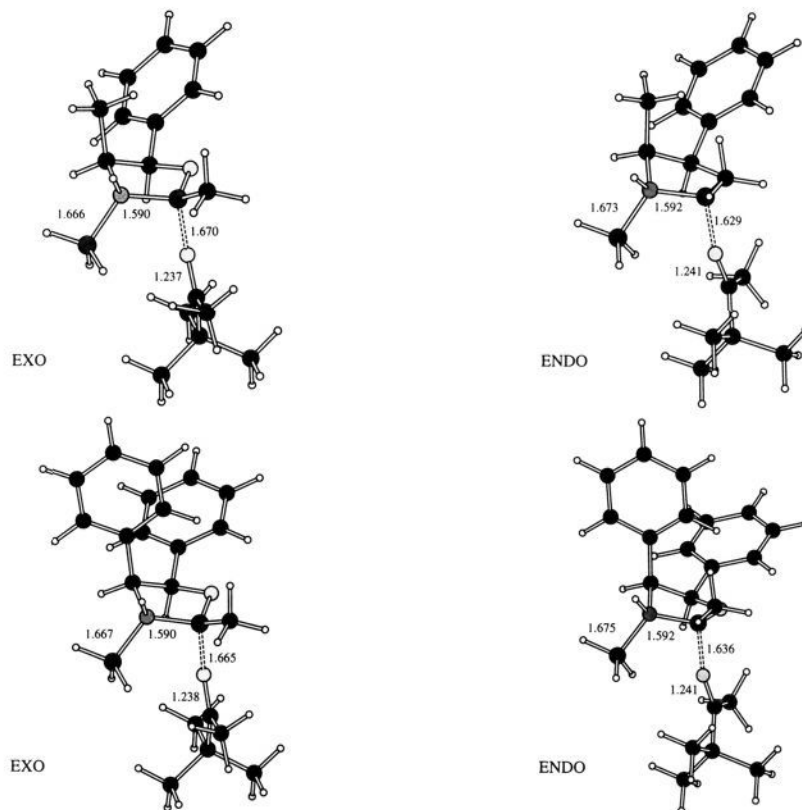
Figure 2. 3-21G-optimized geometries for the *exo* (left) and *endo* (right) complexes of *tert*-butyl methyl ketone with the borane adducts of **6** (top) and **7** (bottom).

Chart 1
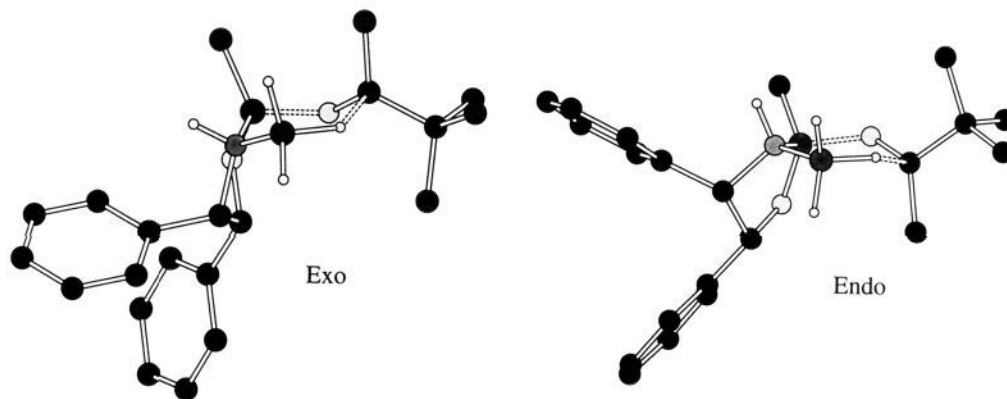
exploratory 3-21G, 6-31G(d), and MP2/6-31G(d) optimizations on a model oxazaborolidine–ketone system were investigated. The model catalyst **21**, an erythro dimethyl analog of **6**, was chosen entirely for computational convenience, and acetone was selected as a prototypical ketone. While the MP2/6-31G(d)//MP2/6-31G(d) level is clearly advantageous for obtaining energetic and geometrical parameters, it is currently not practical for routine application to systems involving **6** or **7**. Through systematic investigation of the model system at the above levels of theory, we should be able to gauge the accuracy of the lower level calculations for the present series of oxazaborolidine catalysts. The optimized geometries for the model catalyst and corresponding *trans* borane adduct are illustrated in Figure 3. The coordination energy of borane to the model oxazaborolidine is computed to be –23.08 kcal/mol at the 3-21G//3-21G level. As found above, this coordination energy is nearly halved to –14.51 kcal/mol at the 6–31G(d)//6-31G(d) level. At the fully correlated MP2/6-31G(d)//MP2/6-31G(d) level, the coordination energy is predicted to be –29.03 kcal/mol. The trends in

borane coordination are very similar to those observed with actual systems previously described and also reflect the sensitivity of the energetics to the level of theory employed. Compared to those of oxazaborolidine **6**, complexation energies obtained for the model system, at comparable levels of theory, differ by less than *ca.* 1 kcal/mol. The geometries of the model oxazaborolidine and borane adduct seem to be equally well represented at all levels of theory studied.

Turning to model catalyst **21** complexation of acetone, again no complexes were located at the 6-31G(d)//6-31G(d) level of theory. However, as speculated above, ketone complexes were identified at the MP2/6-31G(d)//MP2/6-31G(d) level as well as at the 3-21G//3-21G level (Figure 4). Thus, when investigating these systems with basis sets augmented by polarization functions, a correlation energy correction must be included in the geometry optimization. The intrinsic driving force for *endo* complexation of acetone at the MP2/6-31G(d)//MP2/6-31G(d) level is preferred by 2.01 kcal/mol over the *exo* complex. The preference for *endo* complexation of acetone is predicted to be larger at the
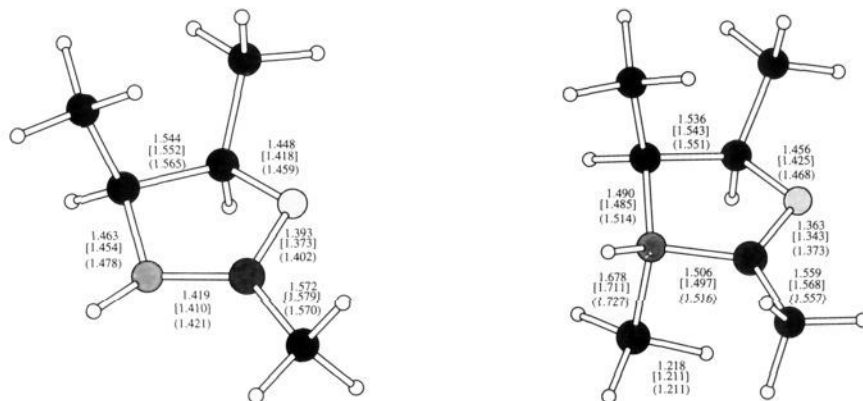
Figure 3. MP2/6-31G(d), 6-31G(d) (in brackets), and 3-21G (in parentheses), optimized geometries for the model oxazaborolidine **21** and borane adduct.
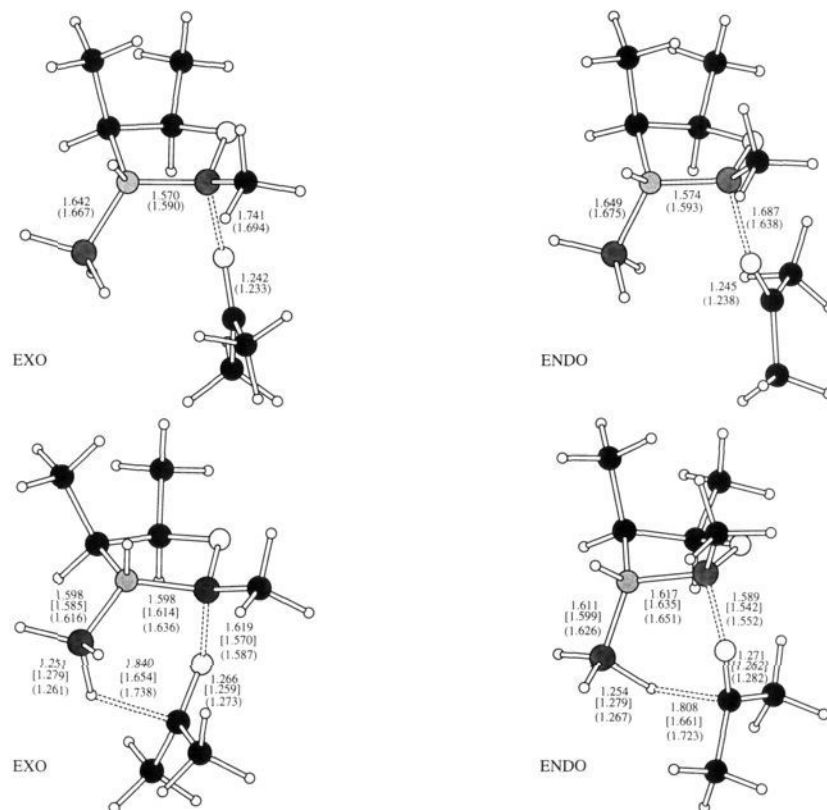
Figure 4. MP2/6-31G(d), 6-31G(d) (in brackets), and 3-21G (in parentheses) optimized geometries for the *exo* (left) and *endo* (right) complexes and transition states of the model catalyst **21** with acetone.

3-21G//3-21G level (3.32 kcal/mol) but is still in reasonable accord with the fully correlated results. Prior ab initio calculations on the complexation of formaldehyde to a model oxazaborolidine catalyst also predict a favored *endo* conformation (0.96 kcal/mol lower in energy).[15i] Relative to the borane adduct, the *endo* complex of acetone to the model catalyst is predicted to be stabilized by –10.11 kcal/mol, comparable to the –13.00 kcal/mol stabilization predicted for the *endo* complex of *tert*-butyl methyl ketone to **6** at the 3-21G//3-21G level. The larger complexation energy of *tert*-butyl methyl ketone to the borane adduct of **6**, relative to the acetone complex in the model system, is due to the greater Lewis basicity of *tert*-butyl methyl ketone relative to acetone.

There appear to be a variety of factors acting in concert to favor the *endo* complexation of acetone to the model catalyst. The B---O=C distance is 1.687 Å for the *endo* complex at the MP2/6-31G(d)//MP2/6-31G(d) level, while the corresponding distance in the *exo* complex is 0.054 Å longer (1.741 Å), indicative

of a weaker complex. At the 3-21G//3-21G level, the B---O=C distances are predicted to be *ca.* 0.048 Å shorter compared to the correlated geometries, but the difference in bond lengths between the *endo* and *exo* complexes is comparable at 0.056 Å. Slight differences are also observed in the B---O=C bond angle between the two complex forms, the *exo* and *endo* angles are computed to be 137.2° and 133.7° at the MP2/6-31G(d)//MP2/6-31G-(d) level. The 3-21G geometries demonstrate the same trend with the bond angles computed to be 143.9° and 137.4°. In each case, a slightly larger bond angle for the *exo* complex of acetone compared to the *endo* is found. A final point worth considering in the complexation of acetone is the conformational change that occurs in the pendant methyl groups. The lowest energy conformation of acetone has the methyl hydrogens eclipsing the C=O bond. In the *exo* complex, the *syn* methyl group of acetone adopts a *gauche* conformation, which is 0.76 kcal/mol higher in energy than the eclipsing conformation at the MP2/6-31G(d)/

/MP2/6-31G(d) level. Again, this is to be compared to the *endo* complex, in which the *syn* methyl group is only slightly rotated (*ca.* 28.5°), at an energetic cost of 0.33 kcal/mol. The larger distance, angle, and twisted conformation of acetone all contribute to the higher energy of the *exo* complex.

The location of the transition states associated with the hydride transfer for the model catalyst are illustrated in Figure 4. As with the complexes described above, we find the *endo* transition state to be the lowest in energy, −29.55 *vs* −28.57 kcal/mol for the *exo* one at the MP2/6-31G(d)//MP2/6-31G(d) level. The 3-21G//3-21G result also establishes the *endo* transition state to be lower in energy (−27.09 *vs* −24.05 kcal/mol). The energy difference between the *endo* and *exo* transition states is 0.98 kcal/mol (MP2/6-31G(d)//MP2/6-31G(d)), compared to the difference found between the two corresponding complexes of 2.01 kcal/mol. It is interesting to find that both the *endo* complex and transition state are lower in energy than the corresponding *exo* form. The overall barrier height, computed from the complex to transition state, for the *endo* pathway is 1.03 kcal/mol higher than the *exo* pathway at the MP2/6-31G(d)//MP2/6-31G(d) level. The preference for the *exo* pathway at the 3-21G//3-21G level is computed to be 0.28 kcal/mol. Clearly, it is the overall barrier height that will ultimately determine the preferred pathway.

The important components of the transition state combine to form a six-membered ring, defined by the carbonyl C=O, oxazaborolidine B—N, and borane adduct B—H units. Corey has hypothesized that the hydride transfer occurs through a boat-like transition state. In the *endo* transition state, these units do form a "boat-like" arrangement; however, the *exo* transition state is best characterized as "chair-like" for the model system (Figure 4). Jones and Liotta also found a chair transition state to be the most favored in a semiempirical study of various CBS catalysts.[16] In comparing the geometries of the transition states obtained at the 3-21G and MP2/6-31G(d) levels, the 3-21G result tends to overestimate the covalent bond distances and to underestimate the complexation and hydride transfer distances relative to the correlated results. The same trend in bond distances is also observed for the acetone complexes with the borane adduct. As the transition state is formed, the geometry of the acetone molecule is significantly distorted from planarity toward a more tetrahedral structure. For both the *endo* and *exo* transition states, the CCCO dihedral angle of acetone is computed to be 156.4° at the MP2/6-31G(d)//MP2/6-31G(d) level. It is noteworthy that in the preferred *exo* pathway, the H---C hydride transfer distance is slightly longer than the corresponding distance in the *endo* transition state (*ca.* 0.032 Å at the MP2/6-31G(d)//MP2/6-31G(d) level). Moreover, on going from the complexes there are small changes in the B---C=O bond lengths for the *endo* and *exo* transition states. In the *endo* transition state, this bond distance is 1.589 Å, which is 0.098 Å shorter than that in the complex (MP2/6-31G(d)//MP2/6-31G(d)). A similar, but more pronounced decrease in bond length is observed for the *exo* transition state, computed to be 0.122 Å shorter than that in the complex. A decrease in the B---C=O angle is also predicted for both transition states, with the *endo* and *exo* angles computed to be 125.9° and 128.2° at the MP2/6-31G(d)//MP2/6-31G(d) level. As the acetone molecule pyramidalizes and moves closer to the borane unit in the transition state, there is a pronounced deformation in the oxazaborolidine ring. This is reflected in the positioning of the borane unit; the torsion about the complexed nitrogen (C4–N3–B2–BH₃ dihedral) increases to −132.6°, from −119.3° in the borane adduct, in the *exo* transition state MP2/6-31G(d)//MP2/6-31G(d). There is a less pronounced shift in the *endo* transition state (−125.3°), owing to the fact that the acetone molecule is complexed more closely to the oxazaborolidine ring.

Unlike the investigation of the complexes, transition states

were located at the 6-31G(d)//6-31G(d) level (Figure 4). Since we have established the borane–adduct ketone complexes as key intermediates on the reduction pathway, critical for the proper energetic description of the reduction process, the 6-31G(d)//6-31G(d) results will not be discussed further, but they are provided for comparative purposes. On the basis of the MP2/6-31G(d)//MP2/6-31G(d) benchmark calculations, the 3-21G//3-21G level appears to be a reasonable level of theory to investigate this series of oxazaborolidine catalysts.

4. Transition States. Returning to the actual systems of interest, the structures of the transition states corresponding to the *exo* and *endo* approach of *tert*-butyl methyl ketone to **6** and **7**, optimized at the 3-21G and 6-31G(d) levels, are illustrated in Figure 5. As found for the model system, the *endo* transition state of **6** is 2.18 kcal/mol lower in energy than the *exo* transition state. The preference for the *endo* transition state involving **7** is diminished to 0.14 kcal/mol. For catalyst **7** the experimental ee is 88% with *tert*-butyl methyl ketone. This corresponds to a free energy difference of 1.63 kcal/mol favoring the *exo* pathway. For catalyst **6** the experimental ee is 82%, which gives rise to a free energy difference of 1.37 kcal/mol. At the 3-21G level we predict a 2.08 kcal/mol preference for the *exo* pathway for **7** and a 1.34 kcal/mol preference for **6**, in good accord with the experimental results. In each case, the calculations correctly establish the preferred product for catalysts **6** and **7**. Previous observations regarding the geometries of the model transition states apply equally well to these systems. The *endo* transition state of **6** has shorter B---C=O bond distances than the *exo* one (1.549 *vs* 1.575 Å) and slightly smaller B---C=O angles as well (130.4° *vs* 132.4°). For the equivalent comparisons with the transition states of **7**, bond distances of 1.549 *vs* 1.572 Å and bond angles of 130.7 *vs* 132.5° are predicted. In each case, the hydride transfer distance is found to be slightly larger for the *exo* transition states than the *endo* transition states. Additionally, the six-membered ring, formed by the previously described units, displays two characteristic features: the first is a distortion of the *tert*-butyl methyl ketone, which is *ca.* 23–25° out of plane, and the second is a more pronounced twisting of the oxazaborolidine ring in the *exo* transition states. Again, the *exo* transition states show a C4–N3–B2–BH₃ dihedral angle of *ca.* −133°, while the *endo* transition states are closer to −124°, with the parent borane adducts of **6** and **7** giving rise to a dihedral angle of 119.8°. A "chair-like" transition state is predicted for both the *exo* and *endo* species. The similarities among all the corresponding systems (*e.g.*, the borane adducts, ketone complexes, and transition states) studied supports the use of the 3-21G//3-21G level of theory in evaluating the catalytic reduction mechanisms of these oxazaborolidines.

Our initial hypothesis was that the "large" and "small" groups attached to the ketone determined the mode of complexation to the borane adduct, due to steric clashes with the substituent on the oxazaborolidine boron. However, the results of the calculations suggest that the inherent preference for the *exo* pathway plays an important role in determining the observed enantioselectivity. If steric repulsion between the boron substituent and the "large" group of the ketone were a major determinant in the mode of complexation, one would anticipate the *endo* complexes and transition states to be higher in energy than the *exo* forms. The opposite is observed, with both *endo* complexes and transition states predicted to be lower in energy. This is consistent with the relative lack of enantioselective sensitivity displayed by various boron substituents in catalysts **7–10** (*cf.* Table 1). Steric repulsion is important in the preference for *anti* complexation of ketones, with respect to the "large" group, to the Lewis acid, which ultimately determines the nature of the product.

5. N-Alkyl Substitution. With the present theoretical results in hand, an explanation of the diminished enantioselectivity displayed by N-alkyl substitution, specifically catalyst **11**, was
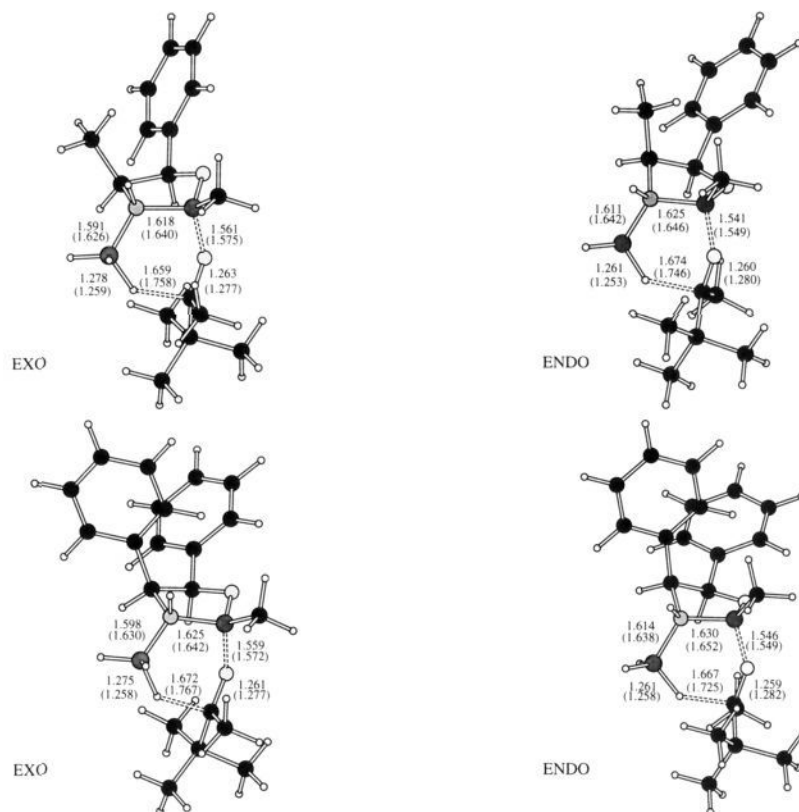
Figure 5. 6-31G(d) and 3-21G (in parenthesis) optimized geometries for the *exo* (left) and *endo* (right) transition states of **6** (top) and **7** (bottom) with *tert*-butyl methyl ketone.
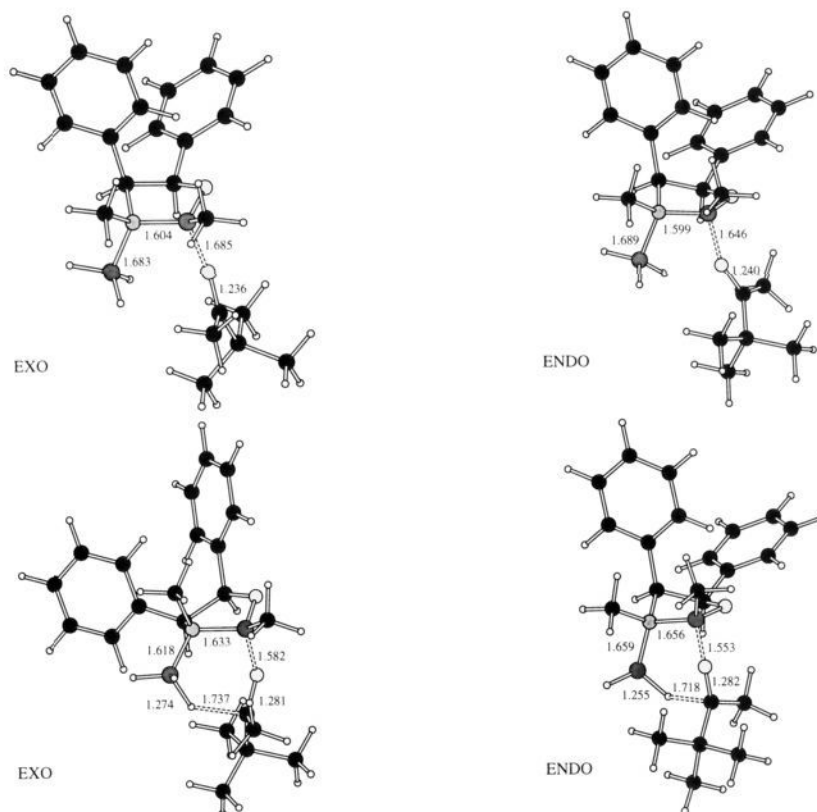
Figure 6. 3-21G-optimized geometries for the *exo* (left) and *endo* (right) complexes and transition states of the catalyst **11** with *tert*-butyl methyl ketone.

sought. One preceding proposal was that retarded formation of the borane adduct led to an increase in uncatalyzed reduction of the ketone by free borane. Supporting this explanation, *trans*

coordination of borane to **11** is predicted to be less favorable than the analogous coordination of borane to **7**, −19.6 *vs* −21.7 kcal/mol, respectively (3-21G//3-21G level of theory used exclusively

Synthetic and ab Initio Study of Chiral Oxazaborolidines

J. Am. Chem. Soc., Vol. 116, No. 19, 1994 8525

herein). Again, *trans* coordination of borane to **11** is preferred over *cis* by 10.76 kcal/mol. Since borane coordination is still predicted to be favorable, though somewhat less, attention turned to the transition states. Examination of the C4'–C4–N3–H$_{N4}$ dihedral angle (C4' refers to the carbon substituent attached to C4) in the *exo* and *endo* transition states for **7** (Figure 5) reveals a more eclipsed conformation for the *exo* transition state (1.6°) as compared to the *endo* (27.9°). This eclipsed conformation is caused by the envelope of the five-membered oxazaborolidine ring (C5–C4–N3–B2 dihedral angle) adopting a more planar configuration in the *exo* transition state (13.8°), while the *endo* angle is computed to be 39.0°. One would expect unfavorable nonbonded interactions between a methyl group on nitrogen and the proximal substituent on carbon to impact the *exo* transition state more than the *endo* one, as is evident from inspection of Figure 5. This was tested by location of the complexes and transition states associated with the reduction of *tert*-butyl methyl ketone by **11**, illustrated in Figure 6. Experimentally, the reduction of α-tetralone by **11** (using a stoichiometric amount of oxazaborolidine) gives 30% ee. This translates into a free energy difference between the *exo* and *endo* pathways of 0.37 kcal/mol favoring the *exo* pathway, assuming only catalyzed reduction occurs. As above, the barrier heights were computed for the reduction of *tert*-butyl methyl ketone. The trends observed in the computations should be comparable to the experimentally determined reduction of α-tetralone (Table 1). Computation of the overall barrier heights yields a 0.79 kcal/mol preference for the *exo* pathway for the reduction of *tert*-butyl methyl ketone by **11**. Comparison of the barrier heights for the *exo* transition states of **7** and **11** shows that N-methyl substitution raises the barrier of **11**, relative to **7**, by 2.44 kcal/mol, while the *endo* barrier for **11** is raised by only 1.15 kcal/mol in comparison to **7**. Alkyl substitution on the oxazaborolidine nitrogen tends to affect the *exo* transition state more than the corresponding *endo* transition state; the net result is a decrease in the predicted enantioselectivity. This effect will be more pronounced for catalysts with larger substituents on C4, which is demonstrated by comparison of **11** and **4** (Table 1). Thus, the decrease in enantioselectivity for the *N*-alkyl-substituted oxazaborolidines can be traced to the *exo* transition state.

The unique striking conformational change in the *exo* transition state of **11** (Figure 6), in comparison to **7**, results from the unfavorable nonbonded interactions between the *N*-methyl substituent and the proximal (C4) phenyl group. The envelope of the five-membered oxazaborolidine ring has "flipped", relative to previous conformations, forcing the phenyl substituent into a higher energy configuration in order to accommodate the geometric requirements of the *exo* transition state. The ring envelope for the *exo* transition state of **11** (C5–C4–N3–B2 dihedral angle) is computed to be −27.6°, while the C4'–C4–N3–H$_{N4}$ dihedral angle is −46.1°. For comparison, the same dihedral angles are computed to be 40.7° and 36.4°, respectively, for the *endo* transition state. Thus, significant loss of enantioselectivity can be accounted for by the conformational change that occurs in the *exo* transition state.

All of the synthetic results can be readily understood with the present theoretical treatment. Effectively blocking one face of the oxazaborolidine, in conjunction with molecular recognition

of borane and the ketone carbonyl group by the catalyst, results in high ee. Substitution on nitrogen in the erythro oxazaborolidines (**4, 11**) is detrimental because the formation of the catalyst–borane complex gives rise to unfavorable nonbonded interactions between the R group on nitrogen and the proximal substituent on carbon (C4). These unfavorable interactions increase from norephedrine/ephedrine (Table 1, catalysts **6** and **4**) to the erythro diphenyl N–H/N–CH₃ (catalysts **7** and **11**) derived oxazaborolidines, such that the catalyzed path is overridden by the noncatalyzed borane reduction and competition from the *endo* transition state in the latter. By contrast, the trisubstituted amine in the CBS catalysts **2** readily forms the borane complex due to pyramidalization of nitrogen imposed by the [3.3.0] ring system. Thus, the geminal diphenyl substitutions in **1** and **2** function by placing the phenyl group *cis* to the isopropyl or pyrrolidine ring, which blocks one face of the catalyst. This effect is achieved by the erythro catalysts **7–10** wherein the two phenyl groups, orthogonal to the oxazaborolidine ring, synergistically augment their steric requirements. The second phenyl group in **1** and **2**, *trans* to the isopropyl group or pyrrolidine ring, is either not required or functions to provide additional nonbonded interactions with the ketone to enhance the enantioselectivity. Thus, less than absolute enantioselectivity in the oxazaborolidine-catalyzed reduction can be attributed to at least two variables: noncatalyzed borane reduction[34] and competition from the *endo* transition state. The intrinsic power of molecular recognition by the oxazaborolidine catalysts in the enantioselective ketone reductions is evident from structurally simple erythro substituted oxazaborolidines.

Conclusion

An understanding of the relationship between oxazaborolidine structure and the enantioselectivity obtained in prochiral ketone reductions has been presented. The primary requirement for a good catalyst is a blocked face. Two-point binding of borane and the ketone carbonyl group on the catalyst then occurs to give high ee unless borane coordination forces nonbonded interactions between the nitrogen and proximal carbon substituents. These nonbonded interactions slow the rate of borane coordination, resulting in noncatalyzed borane reduction and competition from the *endo* transition state effectively competing or surpassing the rate of the *exo*-catalyzed path. Thus the molecular recognition of borane and the ketone carbonyl group by an appropriately substituted oxazaborolidine is the key element in the enantioselective reduction. The calculated structures, energetics, and the existence of key intermediates are sensitive to the level of theory applied. The present level of ab initio results at the 3-21G//3-21G level, validated by comparisons with the fully correlated MP2/6-31G(d)//MP2/6-31G(d) level, correctly predicts the relative enantioselectivities in this series of oxazaborolidines. Additionally, the first examples of ab initio transition states are best described as "chair-like" for the preferred *exo* reduction pathway. Diphenyl oxazaborolidines (catalysts **7–10**, Table 1) possess the attributes important for an efficient catalyst, and high enantiomeric excess is achieved.

---

(34) Noncatalyzed borane reduction occurs due to slower rate of borane coordination to the catalyst (as exemplified for **4** and **11**) and ketone complexation to the catalyst. Aliphatic ketones typically give higher ee when erythro-substituted catalysts are increased from 5 mol % to 10 mol %. Aromatic ketones which are more Lewis basic do not show this trend.